PHYSICS AND CHEMISTRY OF SOLID STATE
V. 22, No. 4 (2021) pp. 734-741
Section: Chemistry

DOI: 10.15330/pcss.22.4.734-741

Vasyl Stefanyk Precarpathian National University

ФІЗИКА І ХІМІЯ ТВЕРДОГО ТІЛА
Т. 22, № 4 (2021) С. 734-741
Хімічні науки

PACS: 68.55.Ln ISSN 1729-4428

Abdelmalek Kharroubi[1], Aboulkacem Khiali[1], Hadj Benhebal[2],*, Bedhiaf Benrabah[1], Salima Lellou[3], Samir Kadi[3] and Bellal Sadouki[1]

Synthesis and Properties of (Bi, Cd)-doped $CuMn_2O_4$ thin films by sol-gel dip-coating method

[1]Laboratory of Physical Engineering, University of Tiaret, Tiaret (14000), Algeria,
[2]Department of Chemistry, Faculty of Material Sciences, University of Tiaret, Tiaret (14000) Algeria. benhebalh@yahoo.dz
[3]Laboratory of Plant Physiology Applied to Above-Soil Culture, Department of Nature and Life Sciences, University of Tiaret, Tiaret (14000) Algeria.

In the present experimental research work, thin films of pure and (Bi,Cd)-doped $CuMn_2O_4$ have been deposited onto pyrex glass substrates at optimized substrate temperature of 500°C, using sol-gel dip-coating method. The copper nitrate, manganese nitrate, bismuth nitrate and cadmium nitrate were used as precursor materials with distilled water as solvent. Deposited thin films were studied using X-ray diffraction, absorption UV-Vis spectroscopy, Fourier transform infrared spectroscopy (FTIR) and impedance spectroscopy. The X-ray diffraction pattern indicated a copper manganite ($CuMn_2O_4$) spinel structure. The crystallite size determined using Debye-Scherrer's formula, increased with increasing the Bi and Cd concentration and found in the range of 19,46-52,32 nm. FTIR spectrum depicted the presence of two distinct bands at 663.5 cm-1and 567 cm-1 characterizing $CuMn_2O_4$ spinel-type structure. Thin films have the best absorbance in the ultra-violet and blue regions. The highest absorbance observed was for the Cd-doped sample at 6%. Moreover, the optical energy band gaps (Eg) of deposited thin films determined by Tauc's relation decreases with addition of Bi and Cd content. The impedance spectra (Nyquist plots) of the films show semicircle arcs and the electrical resistance of the thin films was reduced from 81.6 to 31.20 Ω for the doped Bi and from 81.6 to 43.62 Ω for the doped Cd. An RC electrical equivalent circuit can be proposed. Thus, our results indicate the possibility of developing semiconductor materials with a spinel structure having interesting optoelectrical properties for different technological applications.

Keywords: Thin films, Sol-gel, $CuMn_2O_4$, Bismuth, Cadmium

Received 18 July 2021; Accepted 15 November 2021.

Introduction

Materials based on transition elements with a spinel structure exhibiting semiconductor properties have already been the subject of a great deal of work, both at the fundamental and applied level, but they continue to generate a great deal of interest in the fields of catalysis and photo catalysis. In recent years the science of nanomaterials and nanotechnologies has emerged as one of the most attractive fields both fundamentally and technologically due to the wide range of possible applications.

In particular, transparent conductive oxides (TCO) have generated considerable interest in the research community due to their intriguing properties; they combine electrical conductivity and optical transparency in the visible range. TCOs are of great interest for many potential applications affecting a wide variety of fields [1].

The multivalent nature of Mn and Cu in $CuMn_2O_4$ structure makes them suitable candidates for engineering applications, In addition, the orientation of the site of Mn and Cu in $CuMn_2O_4$ has an important role in its properties. The distributions of Cu_2 + and Mn_3 + in CuMn2O4 structure are in tetrahedral and octahedral sites, respectively, which are known as normal spinel

structures; the corresponding general formula is written as AB_2O_4 [2-5].

In this type of material has aroused great interest for their diverse properties such as electrochemical, photocatalytic, magnetic properties, sensor and lithium-ion batteries. The spinel type of ternary manganese oxides like $NiMn_2O_4$, $CoMn_2O_4$, $CuMn_2O_4$ and $ZnMn_2O_4$ have been recently investigated and reported [6-11]. $CuMn_2O_4$ nanostructures have semiconductor properties and can be used in the electronics industry, There are several methods of preparing nanostructures such as the combustion method [12], Soft reactive grinding [13], Chemical vapor deposition [14], Solid-state reaction [15], hydrogen storage[16], hydrothermal method[17], Sol-gel[18], atomic layer deposition [19].

We are interested in the synthesis by the Sol-gel process of thin layers based on $CuMn_2O_4$. This relatively recent method, making it possible to produce oxide materials (glasses, ceramics, etc.). The use of very pure chemical reagents guarantees the purity of the materials synthesized. The stoichiometry of the different chemical elements can be easily checked by mixing the different precursors in the initial solution. The low viscosity (in general) makes it possible to obtain good homogeneity at the molecular level [20,21].

I. Experimental procedure

1.2. Synthesis

The materials were developed by the sol-gel Dip-coating method. The synthesis protocol adopted for the preparation of the solutions was inspired from the work carried out by M. Pengjun et al [6] and M. Kramer et al [18].

$CuMn_2O_4$ solutions are obtained by mixing two types of preparations. The first solution is obtained by dissolving copper (II) nitrate trihydrate (Sigma Aldrich, 98%) in distilled water. Magnetic stirring for 1 hour results in the formation of a blue solution. The second is a solution of manganese (II) obtained by dissolving manganese nitrate tetrahydrate (Sigma Aldrich, 98%) in distilled water. After mixing the two solutions, an ethanolic solution of citric acid (Janssen, purity> 99%) was added drop wise. The mixture is slowly heated at 80°C for 2 hours with magnetic stirring; this solution is characterized by a blue color (solution three). (Bi and Cd)-doped $CuMn_2O_4$ solutions were prepared using Bismuth (III) nitrate pentahydrate (Merck, 71%) and Cadmium (II) nitrate tetrahydrate (Biochem, 99%) dissolved in ethanol (Sigma Aldrich, 99.8%) and stirred for 2 hours. The obtained solution is transparent, blue in color and slightly viscous. Appropriate volumes of the doping solutions were taken and added to the corresponding volumes of solution three in order to obtain a doping rate (6 and 9%). the mixtures thus obtained were stirred and then dip-coated on pyrex glass substrates (25mmx75mmx1 mm) at a drawing speed of 50 mm/min. Then the layers were dried at 100° before being heat treated at 500°C. This protocol is well detailed in Fig 1.

1.2. Characterization

The structural characterization of the powders was analyzed using a Philips PW1830 X-ray diffractometer

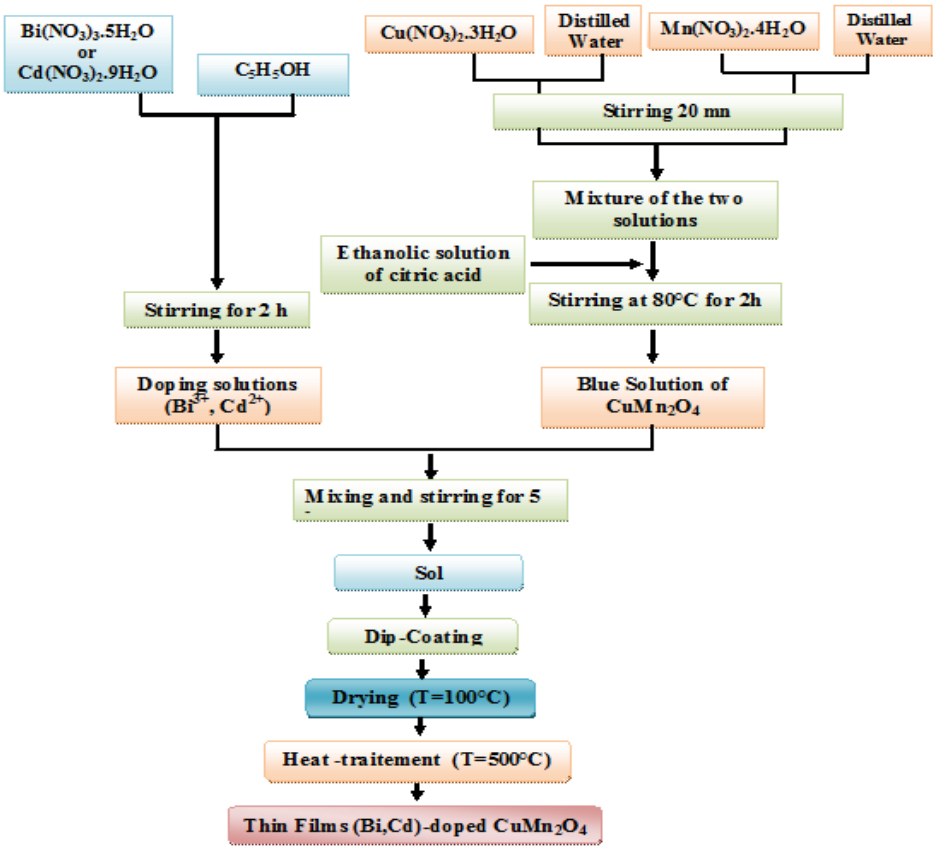

Fig. 1. Schematic diagram of sol–gel synthesis of undoped and (Bi,Cd)-doped $CuMn_2O_4$.

with (CuKα) radiation using a copper anticathode (I = 30 mA; V =40KV; λ = 1.5406 Å). The optical transmittance of the films was measured using UV-1650 Shimadzu spectrophotometer in the wavelength range from 300 to 900 nm. FTIR spectra of the samples were recorded using a Shimadzu 8400 Spectrometer in the wave number range from 400 cm-1 to 4000 cm-1. Impedance measurements were performed using the Agilent4284A LCR meter operating in the frequency range 75 kHz to 20 MHz with oscillation amplitude of 1 V.

II. Results and discussion

2.1. Structural properties

Fig. 2 shows identification by X-ray diffraction of the crystalline phases in the various samples of the spinel oxides $CuMn_2O_4$ and (Bi,Cd)-doped $CuMn_2O_4$ at.6 and 9%, synthesized by the sol-gel technique. From diffractograms (Fig.2), both $CuMn_2O_4$ (JCPDS No. 74-2422) [6,22] and Mn_3O_4 (JCPDS card No. 24-0734) [23] spinel phases can be seen, but $CuMn_2O_4$ is dominant. In addition, the XRD patterns of the samples showed a minor amount of Mn_2O_3 crystalline phase (JCPDS card No 41.1442) [24].

No notable diffraction peak due to the CuO phase could be distinguished. The absence of the CuO related peaks suggests that; either the amount of CuO formed is too small to be detected by XRD, or the Cu specie entered the spinel structure of Mn_3O_4 and replaced Mn to occupy the tetrahedral position and formed the $CuMn_2O_4$.

An additional peak appeared at 2θ=28° on the diffractogram of the sample doped Bi (at.9%) that could be attributed to the lattice plane (120) of Bi_2O_3 phase [25].

With the doping of $CuMn_2O_4$, the peak of the spinel phase begins to become less intense, while that of the Mn_2O_3 phase intensifies more as the doping rate increases. This may be due to the deterioration of the crystal structure of $CuMn_2O_4$ following the incorporation of the dopants Bi^{3+} and Cd^{2+} having ionic radii higher than those of copper and manganese [26].

The grain size of $CuMn_2O_4$ and (Bi,Cd)-doped $CuMn_2O_4$ samples have been calculated using the following Scherrer's formula using the maximum intense peaks (311) and (000) [27,28]:

$$\tau = \frac{0.9\lambda}{\beta \cos(\theta)}, \quad (1)$$

Where: λ is The wavelength of the X-ray radiation (λ CuKα = 1.5406 Å),: β is the the width at mid- at half maximum (FWHM) diffraction peak, θ: The diffraction angle (degree).

From the table 1, The average grain size of the samples varies from 19,46 nm for Undoped-$CuMn_2O_4$ to 52,32 nm for the Cd-doping at 9%.

2.2. Fourier transforms infra-red spectroscopy:

The CuMn2O4 thin-film samples produced by combined methods (sol-gel@Dip-coating) and doped with Bi and Cd at 6 and 9%, were subjected to FTIR analysis at room temperature to evaluate the chemical composition and to confirm the formation of the crystalline phase of the oxide. The infrared spectra of all samples recorded in the range 400 to 4000 cm-1 are shown in Fig 3. The two prominent, strong and characteristic bands appearing at approximately 567 cm^{-1} and 663.5 cm^{-1} indicate the formation of metal-oxygen bands [29]. The first around 567 cm^{-1} indicates the presence of vibrational stretching mode of manganese (Mn^{3+}–O^{2-}) in the tetrahedral sites [30]. The second at

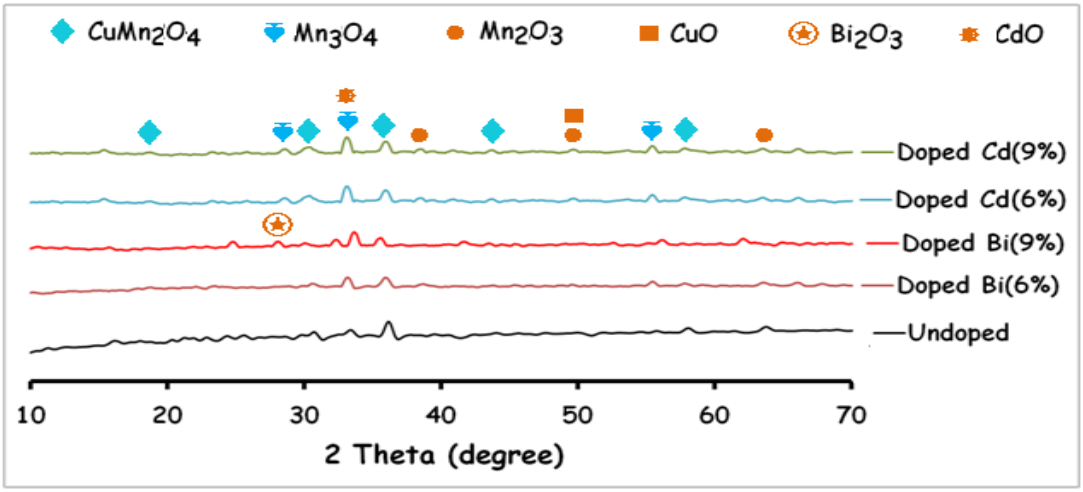

Fig. 2. XRD patterns of undoped and (Bi,Cd)-doped $CuMn_2O_4$ samples.

Table 1

Crystallite sizes of undoped and (Bi,Cd)-doped $CuMn_2O_4$.

Sample	Undoped $CuMn_2O_4$	$CuMn_2O_4$: Bi (6 %)	$CuMn_2O_4$: Bi (9 %)	$CuMn_2O_4$:Cd (6 %)	$CuMn_2O_4$:Cd (9 %)
Crystallite sizes **τ** (nm)	19.464	31.734	45.761	33.252	52.322

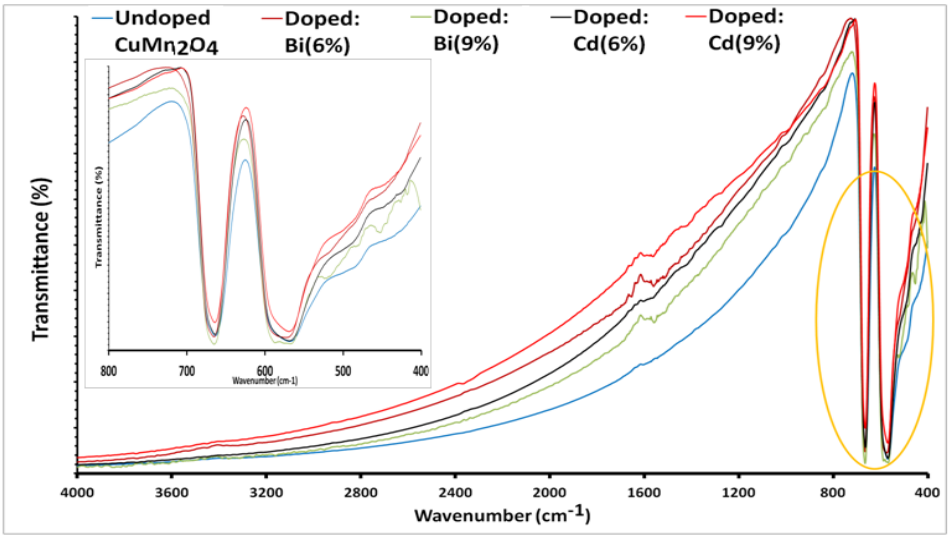

Fig. 3. FTIR spectra of undoped and (Bi,Cd)-doped $CuMn_2O_4$ films.

663.5 cm-1 bound to the spinel $CuMn_2O_4$ which reveals the formation of spinel nanoparticles with good crystallinity [31]. The small peaks at 995 cm-1 and 1600 cm-1 are associated with the presence of moisture absorbed on $CuMn_2O_4$ samples [32].

2.3. UV–Visible spectroscopy

Fig. 4 shows the transmission spectra of undoped $CuMn_2O_4$ and Bi-Cd-doped $CuMn_2O_4$ thin films for different doping rates (6%, 9%). The films exhibit good transparency in the visible 75% - 95%, which varies slightly with Bi and Cd doping. This indicates a good optical quality of the deposited layers and shows a negligible effect of light scattering and / or losses due to absorption. The transmission spectra show two regions: A region of good transparency over a wide wavelength range from 400 to 900 nm, this high transparency is one of the properties that explain the interest in thin films of $CuMn_2O_4$ as a transparent conductive material. A region of high absorption (λ <350 nm), which is due to the absorption of radiation by free charge carriers in the film, by inter-band electronic transitions, The variation in transmission in this region is used to determine the optical gap.

The optical gap (Eg) of the samples can be obtained from the transmission spectrum using the Tauc relation. Indeed, the transition of an excited electron from the valence band to the conduction band corresponds to the energy gap of the semi-conductor band gap.

For crystalline materials, the absorption coefficient (α) as a function of the energy of the photon (hν), in the case of a direct transition, is expressed by the following relation [33,34].

$$(h\nu) = A^*(h\nu - E_g)^2, \quad (2)$$

Where: A* is a constant and α is the optical absorption coefficient. If we express the transmittance T in (%), the absorption coefficient is given by:

$$\alpha = \frac{1}{d}.ln\left[{}^{100}/_{T(\%)}\right], \quad (3)$$

The values of the optical gap as translated by Fig. 5, are determined for each sample by plotting (αhν)2 as a function of (hν) and by extrapolation of the linear region

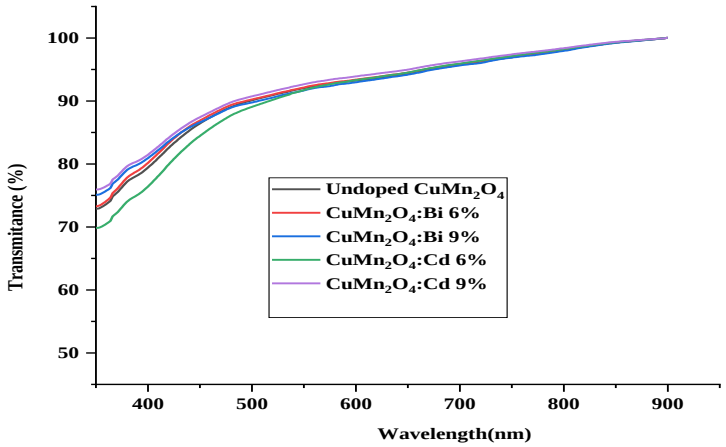

Fig. 4 UV–visible spectra of undoped and (Bi,Cd)-doped $CuMn_2O_4$ films.

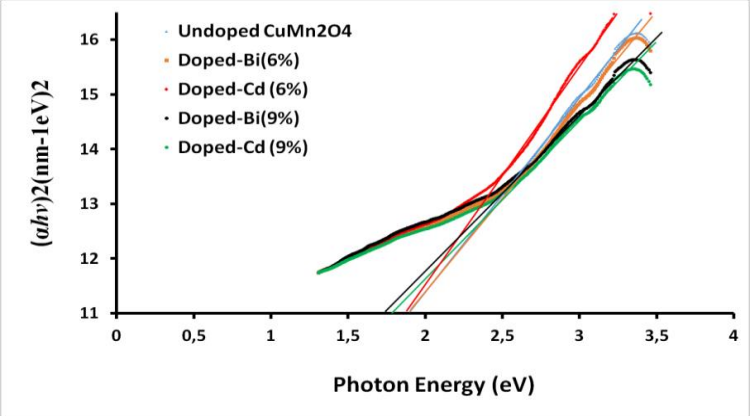

Fig. 5. Tauc plots of undoped and (Bi,Cd)-doped $CuMn_2O_4$.

Table 2

Values of optical gap undoped and (Bi,Cd)-doped $CuMn_2O_4$.

Sample	Undoped $CuMn_2O_4$	$CuMn_2O_4$: Bi (6 %)	$CuMn_2O_4$: Bi (9 %)	$CuMn_2O_4$:Cd (6 %)	$CuMn_2O_4$:Cd (9 %)
Eg (eV)	1.9	1.86	1.64	1.83	1.77

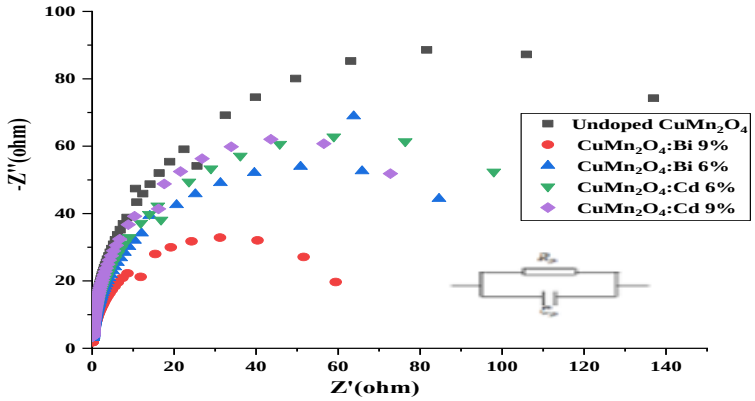

Fig. 6. Nyquist representation of impedance of undoped and (Bi,Cd)-doped $CuMn_2O_4$.

up to (αhν)2=0.

From Table 2, it observed that the optical gap of the films decreases from 1.90e.V for pure $CuMn_2O_4$ up to 1.64e.V for $CuMn_2O_4$ doped with Bi 9% and 1.77 for $CuMn_2O_4$ doped with Cd 9%. This variation of the optical gap as a function of the Bi-Cd doping rate is mainly due to the concentration of free electrons. Therefore, films prepared with different percentages of the Bi and Cd doping contains a high concentration of charge carriers.

2.4. Impedance spectroscopy

The measurement of the electrical properties of materials requires powerful tools to explore the electrical behavior, by modeling them by an equivalent circuit [35]. In this method, we apply a sinusoidal disturbance of constant amplitude and a variable frequency to determine the conduction properties of an oxide and, in theory, the different contributions to the conduction of a material (grains, grain boundaries, pores, and faults) [36-38].

Fig. 6 is Nyquist's presentation of undoped and (Bi, Cd) -doped $CuMn_2O_4$ thin films at 6%, and 9%).

Fig. 6 is the Nyquist representation of thin films of pure $CuMn_2O_4$ and (Bi,Cd)-doped $CuMn_2O_4$, the frequency of which varies from 75kHz to 20 MHz at room temperature. The different processes taking place at the electrode / electrolyte interface can be modeled by constructing an equivalent RpCp electrical circuit. The physical logic of the system indicates that concurrent processes are connected in parallel. The capacitance Cp of thin films was calculated using the following equation [39]:

$$C_p = \frac{1}{2\pi f_c R_p}, \quad (4)$$

Where fc is the frequency of the external applied field at the apex of the circular arc. The resistance Rp was determined by the intersection of the Nyquist plot with the real axis.

This figure is characteristic of a circuit RpCp in parallel, where Cp is the capacity of the layer and Rp its resistance.

Table 3 shows the parameters determined from the

Table 3

Values of fc, R_P and C_P of undoped and (Bi,Cd) doped $CuMn_2O_4$.

Sample	Undoped $CuMn_2O_4$	$CuMn_2O_4$: Bi 6 %	$CuMn_2O_4$: Bi 9 %	$CuMn_2O_4$: Cd 6 %	$CuMn_2O_4$: Cd 9 %
f_c(KHz)	519	519	519	519	519
R_p(Ω)	81.6	50.85	31.20	58.94	43.62
C_p(nF)	3.75	6.02	9.82	5.20	7.02

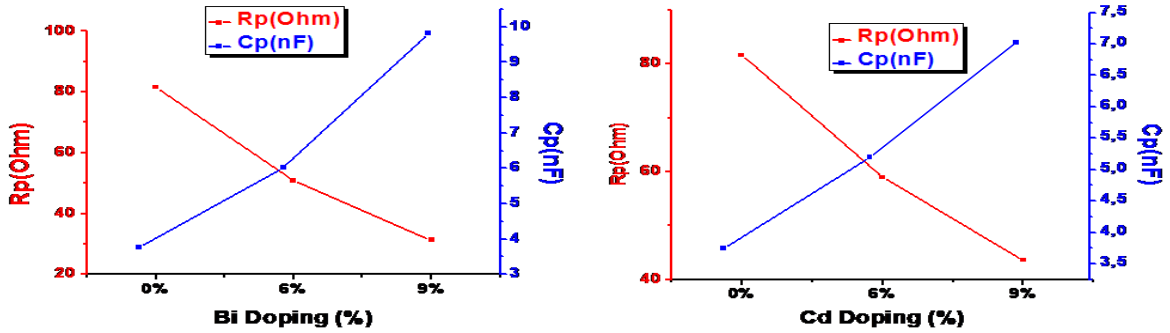

Fig. 7. Variation of RP and Cp as function of Bi and Cd doping level.

analysis of Nyquist diagrams. The above equation (4) allowed us to deduce the value of the capacitance of the $CuMn_2O_4$ layer for different Bismuth and Cadmium doping.

We notice from Fig 7, that the resistance Rp decreases while increasing the doping rate in Bi and Cd and reaches respectively a value of 31.20 Ω and 43.62 Ω for a doping rate of 9%, on the other hand the capacitance increases from 6.02 nF to 9.82 nF for Bismuth and from 5.20 nF to 7.02 nF for cadmium, for the same doping of 9%. The variation of these capacities are possibly linked with the formation of oxygen vacancies, this is due to the substitution of (Cu_2+) by the ions Bi_3+ and Cd_2+ on the grain surface [40].

III. Conclusion

The present work made it possible first of all to adjust the parameters by the sol-gel dip-coating process of undoped and (Bi, Cd)-doped $CuMn_2O_4$ in order to obtain homogeneous $CuMn_2O_4$: Bi and $CuMn_2O_4$: Cd thin films. The results of the X-ray diffraction show that the incorporation of the two dopants prevented the growth of the $CuMn_2O_4$ phase to the detriment of the Mn_2O_3 phase. Even more, the incorporation of Bi^{3+} and Cd^{2+} promotes the formation of agglomerates having a larger average size than in the case of the undoped oxide. For UV-Visible spectroscopy, all the spectra indicate good transmittance (transparency) in the visible range and the optical gap of the $CuMn_2O_4$ layers increases with the decrease in the doping rate from 1.90 eV for the Undoped $CuMn_2O_4$ to 1.64 eV for $CuMn_2O_4$:Bi (9%) and 1.77 eV for $CuMn_2O_4$:Cd 9%. The infrared peaks at 567 cm-1 and 663,5 cm^{-1} indicate the formation of metal-oxygen bands attributed to Mn-O, Mn-O-Mn and Cu-O witch confirm the formation of crystalline phase of $CuMn_2O_4$. The complex impedance spectroscopy indicates that the effect of the grain boundaries is dominant in the conduction mechanism; we also note that the equivalent diagram of the $CuMn_2O_4$ films of each doping is an RC circuit in parallel.

Acknowledgement

The authors would like to extend their thanks to Prof. El-Habib BELARBI as well as all the members of the Synthesis and Catalysis Laboratory of the Faculty of Material Sciences at the University of Tiaret for all the measurements carried out within the framework of this work.

Abdelmalek Kharroubi –HDR. (physics), Teacher researcher.
Aboulkacem Khiali – Doctor of Engineering Sciences.
Hadj Benhebal – Professor, Professor at the Department of Chemistry.
Bedhiaf Benrabah – Professor, Professor at the department of physics.
Salima Lellou– PhD. Candidate (chemistry), Researcher.
Samir Kadi – HDR. (chemistry), Teacher researcher
Bellal Sadouki – Ph.D. Student (Physics).

[1] S. Sohn, Y.S. Han, Transparent conductive oxide (TCO) films for organic light emissive devices (OLEDs). In: S. H. Ko., editors. Organic light emitting diode-material, process and devices. 1st ed. Rijeka, Croatia: InTech, 233 (2011), https://doi.org/10.5772/18545.
[2] D. Shoemaker, P. Li, R. Seshadri, Journal of the American Chemical Society, 131(32), 11450 (2009) https://doi.org/10.1021/ja902096h.
[3] D. Haiwei, Y. Wang, T. Wan, , T. Arandiyan, D. Chu, ACS Applied Energy Materials 1(7), 3035 (2018) https://doi.org/acsaem.8b00548.

[4] P.O. Larsson, A. Andersson, Applied Catalysis B Environmental 24(3-4), 175 (2000) https://doi.org/10.1016/S0926-3373(99)00104-6.
[5] P. Wei, M. Bieringer, L. M. Cranswick, & A. J. Petric, Journal of materials science 40(22), 5821-5828 (2010) https://doi.org/10.1007/s10853 .009.4042.2.
[6] P. Ma, Q. Geng, X. Gao, S. Yang, & G. Liu, Ceramic International, 42(10), 11966 (2016) https://doi.org/1016/j.ceramint.2016.04.122.
[7] N. Senthilkumar, V. Venkatachalam, M. Kandiban, P. Vigneshwaran, R. Jayavel, I. Potheher, Physica E: Low-dimensional Systems and Nanostructures 106, 121 (2019) https://doi.org/0.1016/j.physe.2018.10.027.
[8] P. Vigneshwaran, M. Kandiban, N. Senthil Kumar, V. Venkatachalam,R. Jayave, I. Vetha Potheher, Journal of Materials Science: Materials in Electronics 27(5), 4653 (2016) https://doi.org/10.1007/s10854.016.4343.6.
[9] N. Honghong, M. Wenqin, G. Zhengxiang, G. Baoyou, Z. Xiaojun, RSC Advances 5(31), 24607 (2015) https://doi.org/10.1039/C5RA00979K.
[10] M. Enhessari,A. Salehabadi, A. K. Maarofian, S. Khanahmadzadeh, International Journal of Bio-Inorganic Hybrid Nanomaterials 5(2), 115 (2016).
[11] T. Larbi, K. Doll, M. Amlouk, Spectrochimica Acta Part A: Molecular and Biomolecular Spectroscopy 216, 117 (2019) https://doi.org/10.1016/j.saa.2019.03.022.
[12] S.A. Mirbagheri, S. M. Masoudpanah, S. Alamolhoda, Optik 204(164170), 1 (2020) https://doi.org/10.1016/j.ijleo.2020.164170.
[13] F. Afriani, Ciswandi, B. Hermanto, T. Sudiro, AIP Conference Proceedings. AIP Publishing LLC 216(5), 17 (2018) https://doi.org/10.1063/1.5038298.
[14] K. Suzuki, K. Kazunori, Japanese journal of applied physics 44(4A), 2081 (2005) https://doi.org/10.1143/JJAP.44.2081.
[15] M. Trari, J. Töpfer, P. Dordor, J. Grenier, C. Pouchard, M. Doumerc, Journal of Solid State Chemistry 178(9), 2751 (2005) https://doi.org/10.1016/ j.jssc.2005.06.009.
[16] A.M. Fathi, A. M. Salwa,A.M. Abdel-Hameed, F. H. Margha and A.Nabil, A. Abdel Ghany, Zeitschrift für Physikalische Chemie 230(10), 1519 (2016) https://doi.org/10.1515/zpch-2015-0627.
[17] M. Yoshimura, K. Byrappa, Journal of Materials Science 43(7), 2085 (2008) https://doi.org/10.1007/s10853.007.1853.x.
[18] M.Krämer ,T. Schmidt, K. Stöwe, W.F.Muller, Applied Catalysis A: General 302(2), 257 (2006) https://doi.org/10.1016/j.apcata.2006.01.018.
[19] Y. Lei, J. Lu, X. Luo, T.Wu, P. Du, X. Zhang, K. Amine, Nano. Letters 13(9), 4182 (2013) https://doi.org/10.1021/nl401833p.
[20] L. S. Kaykan, A. K. Sijo, J. S. Mazurenko and A. Żywczak, Applied Nanoscience, (2021) https://doi.org/10.1007/s13204-021-01691-0.
[21] [21] S. Gai, C. Li, P. Yang, J. Lin, Chemical reviews 114(4), 2343 (2014) https://doi.org/10.1021/ cr4001594.
[22] A. Sobhani-Nasaba, M. Eghbali-Arani, S.M. Hosseinpour-Mashkani, F. Ahmadi, M. Rahimi-Nasrabadi, V. Ameri, Iranian Journal of Catalysis, 10(2), 91-99 (2020).
[23] K.A.M. Ahmed, K. Huang, Arabian Journal of Chemistry, 12, 429-439 (2019). https://doi.org/10.1016/j.arabjc.2014.08.014.
[24] A. Khan, H. Wang, Y. Liu, A. Jawad, J. Ifthikar, Z. Liao, T. Wanga and Z. Chen, J. Mater. Chem. A 6, 1590 (2018), https://doi.org/10.1039/C7TA07942G.
[25] Z.A. Zulkifli, K.A. Razak, W.N.W.A Rahman, and S.Z. Abidin, Journal of Physics Conference Series 1082(1):012103 (2018). https://doi.org/10.1088/1742-6596/1082/1/012103.
[26] E.F. Keskenlera, S. Aydin, G. Turgutb and S. Dogan., Acta Physica Polonica A 126 (3), 782 (2014) https://doi.org/10.12693/APhysPolA.126.782.
[27] [A. Monshi, M. Foroughi, M. Monshi, World journal of nano science and engineering 2(3), 154 (2012) https://doi.org/10.4236/wjnse.2012.23020.
[28] A.K. Sijo, Vikash Kumar Jha, Larysa S. Kaykan, and D. P. Dutta, Journal of Magnetism and Magnetic Materials, 497(1) 166047 (2020) https://doi.org/10.1016/j.jmmm.2019.166047.
[29] D. Yuanfu, T. Shidi, Z. Qiumei, S. Zhicong, Z. Leiting, Z. Shuzhong C. Guohua, Journal of Materials Chemistry, 21(32), 11987 (2011) https://doi.org/10.1039/C1JM11575H.
[30] F. Sedighi, A.S. Nasab, M. Behpour, M.R. Nasrabadi, Journal of Nanostructures 9(2), 258 (2019) https://doi.org/10.22052/JNS.2019.02.008.
[31] M.M. Selim, N.M. Deraz, O.I. Elshafey, A.A. El-Asmy, Journal of Alloys and Compounds, 506(2), 541 (2010) https://doi.org/10.1016/j.jallcom.2010.04.180.
[32] P. Zhang, X. Li, Q. Zhao, S. Liu, Nanoscale Research Letters 6(1), 1 (2011), https://doi.org/10.1186/1556-276X-6-323.
[33] A. Kharoubi, A. Bouaza, B. Benrabah, A. Ammari, H. Benhebal, Journal of Molecular and Engineering Materials 6(1), 1 (2018) https://doi.org/10.1142/S2251237318500016.
[34] M. S. Khandekar, N. L. Tarwal, I. S. Mulla, S.S.Suryavanshi, Ceramic International 40(1), 447 (2014) https://doi.org/10.1016/j.ceramint.2013.06.021.
[35] E. K. Lenzi, L. R. Evangelista, L. Taghizadeh, D. Pasterk, R. S. Zola, T. Sandev, I. Petreska, The Journal of Physical Chemistry B, 123(37), 7885 (2019) https://doi.org/10.1021/acs. jpcb.9b06263.

[36] A. Kharoubi, A. Bouaza, B. Benrabah, A. Ammari, A. Khiali, The European Physical Journal Applied Physics, 72(3), 30301 (2015) https://doi.org/10.1051/epjap/2015150282.
[37] B. Benrabah, A. Bouaza, A. Kadari, M. Maaref, Superlattices and Microstructures 50(6), 591 (2011) https://doi.org/10.1016/j.spmi.2011.08.009.
[38] A. Göktaş, A. Tumbul, F. Aslan, Journal of Sol-Gel Science and Technology 78(2), 262 (2016) https://doi.org/10.1007/s10971-016-3960-0.
[39] A. Khiali, A. Ammari, B. Benrabah, A. Bouaza, A. Kharoubi, H. Benhebal , Japanese Journal of Applied Physics 57(4), 5801 (2017) https://doi.org/10.7567/JJAP.57.045801.
[40] R. Muccillo, J. A. Cerri, E. R. Leite, E. Longo, J. A Varela, Materials Letters, 30(1), 125 (1997) https://doi.org/10.1016/S0167-577X(97)80001-8.

А. Харрубі[1], А. Хіалі[1], Х. Бенхебал[2], Б. Бенрабах[1], С. Леллоу[3], С. Каді[3], Б. Садоукі[1]

Синтез та властивості тонких плівок $CuMn_2O_4$, легованих (Bi, Cd), отриманих методом золь-гель покриття

[1]Лабораторія фізичної техніки, Тіаретський університет, Тіарет (14000), Алжир. benhebalh@yahoo.dz
[2]Кафедра хімії, факультет математичних наук, Тіаретський університет, Тіарет (14000) Алжир
[3]Лабораторія фізіології рослин, застосовуваної до надземної культури, Департамент природничих і природничих наук, Тіаретський університет, Тіарет (14000) Алжир

У цій експериментальній роботі наносили тонкі плівки чистого та легованого (Bi,Cd) $CuMn_2O_4$ на підкладки з пірексного скла при оптимізованій температурі підкладки 500°C методом золь-гель нанесення покриття. В якості прекурсорів використано нітрат міді, нітрат марганцю, нітрат вісмуту та нітрат кадмію, а як розчинник – дистильовану воду. Отримані тонкі плівки досліджували за допомогою дифракції рентгенівських променів, абсорбційної UV-спектроскопії, інфрачервоної спектроскопії з перетворенням Фур'є (FTIR) та імпедансної спектроскопії. Рентгенівська дифрактограма вказала на структуру шпінелі міді-манганіту ($CuMn_2O_4$). Розмір кристалітів, визначений за формулою Дебая-Шеррера, збільшувався зі збільшенням концентрації Bi і Cd і знаходився в діапазоні 19,46-52,32 нм. Спектр FTIR показав наявність двох чітких смуг на 663,5 $см^{-1}$ та 567 $см^{-1}$, що характеризують структуру шпінелі $CuMn_2O_4$. Тонкі плівки мають найкраще поглинання в ультрафіолетовій та синій областях. Найвище поглинання спостерігалося для зразка, легованого Cd, при 6%. Крім того, оптична ширина забороненої зони (Eg) нанесених тонких плівок, визначена співвідношенням Таука, зменшується з додаванням вмісту Bi і Cd. Спектри імпедансу (графіки Найквіста) плівок мають форму півкола, а електричний опір тонких плівок зменшено з 81,6 до 31,20 Ом для легованого Bi та від 81,6 до 43,62 Ом для легованого Cd. Запропоновано RC електричну еквівалентну схему. Таким чином, отримані результати свідчать про можливість розробки напівпровідникових матеріалів зі структурою шпінелі з цікавими оптоелектричними властивостями для різних технологічних застосувань.

Ключові слова: наночастинки оксиду металу; фотокаталітична активність; антимікробна активність.